Theoretical analysis of maximum transmit power in a b-modulator

Chimmalgi, Shrinivas; Wahls, Sander

Publication date
2019

Document Version
Accepted author manuscript

Published in
Proceedings 2019 45th European Conference on Optical Communication (ECOC)

THEORETICAL ANALYSIS OF MAXIMUM TRANSMIT POWER IN A b-MODULATOR

*Shrinivas Chimmalgi[1], Sander Wahls[1]**

[1]*Delft Center for Systems and Control, Delft University of Technology, Delft, Netherlands*
**E-mail: s.wahls@tudelft.nl*

Keywords: Fiber nonlinear optics, Optical fiber communication, Limits of optical transmission systems

Abstract

The optimal transmit power in various nonlinear Fourier transform-based transmission systems has been observed to decrease with the signal duration when bandwidth is fixed. A new theoretical explanation for this behavior is provided for a specific b-modulator and validated in simulations.

1 Introduction

The nonlinear Fourier transform (NFT) [1] can solve the normalized nonlinear Schrödinger equation (NSE)

$$i\frac{\partial q}{\partial z} + \frac{1}{2}\frac{\partial^2 q}{\partial t^2} + |q|^2 q = 0, \quad q = q(z,t), \tag{1}$$

which is a model for an ideal lossless single-mode fiber obtained after suitable normalization and path averaging [2, Ch. 5]. Here $q(z,t)$ is the slowly varying pulse envelope, z is the location and t is retarded time, all in normalized units. The nonlinear evolution of the signal along the fiber equals a simple phase rotation in the nonlinear Fourier domain (NFD) [1]. Hence it was suggested to embed data in the NFD and use the NFT to recover the data [3, 4]. This idea is known as nonlinear frequency division multiplexing (NFDM).

NFDM has garnered much attention in recent years and many different NFDM system designs have been proposed [5–8]. A common problem with many NFDM designs is that the optimum transmit power decreases with signal duration, making it difficult to utilize signals significantly longer than the channel memory [9–11]. Thus, signals are typically short with a large portion acting as a guard interval that contains no information, leading to low spectral efficiencies. The difficulties with transmitting longer signals at sufficiently high powers are typically attributed to interactions between the signal and noise during the numerical computation of the NFT [9–12].

In this paper we provide a new explanation for this phenomenon. We derive an upper bound on transmit power for the specific NFDM system proposed in [14]. The bound decreases with signal duration when the bandwidth is kept constant. Since our implementation achieves transmit powers close to that bound, we show that signal-noise interactions are not a major limiting factor in our setup.

2 Review of b-modulation

The NFT is obtained by solving the initial-value problem [1]

$$\frac{\partial \phi(\lambda,t)}{\partial t} = \begin{bmatrix} -i\lambda & q(t) \\ -q^*(t) & i\lambda \end{bmatrix} \phi(\lambda,t), \lim_{t\to-\infty} \phi(\lambda,t) = \begin{pmatrix} e^{-i\lambda t} \\ 0 \end{pmatrix},$$

where z is considered fixed and thus dropped. The Jost scattering coefficients are defined as $a(\lambda) = \lim_{t\to\infty} \phi_1(\lambda,t)e^{i\lambda t}$ and $b(\lambda) = \lim_{t\to\infty} \phi_2(\lambda,t)e^{-i\lambda t}$, where λ is a complex parameter. Information can be embedded in the Jost scattering coefficients in various ways. The NFDM technique in which information is embedded in $b(\xi)$, $\xi \in \mathbb{R}$, is known as b-modulation [13]. The advantages of b-modulation are tight control over signal duration and lower sensitivity w.r.t. noise [11, 13]. For b-modulation the normalized energy $\int_{-\infty}^{\infty} |q(t)|^2 dt$ is equal to [13]

$$E[b(\xi)] = -\frac{1}{\pi}\int_{-\infty}^{\infty} \ln(1-|b(\xi)|^2) d\xi. \tag{2}$$

Power control by constellation reshaping (PCCR): In this paper we analyze the system from [14], where

$$b(\xi) = \sum_{k=-N}^{N} s_k \Psi(\xi - k\Delta_\xi). \tag{3}$$

Here, $\Psi(\xi)$ is a specific flat-top carrier, Δ_ξ is the carrier spacing and the s_k are information symbols. The average signal power is controlled by using a suitably shaped constellation for the s_k. The constellation is shaped such that $\mathbb{E}\{E[s_k\Psi(\xi)]\} = E_d$, where $\mathbb{E}$ denotes expectation w.r.t. the s_k, $E_d > 0$ is a design parameter, and $E[s_n\Psi(\xi)]/E[s_k\Psi(\xi)] = |s_n|^2/|s_k|^2$ for $n \neq k$. This system design ensures that [14]

$$\mathbb{E}\{E[b(\xi)]\} \approx (2N+1)E_d \tag{4}$$

assuming that Δ_ξ is not too small. By definition of the NFT, for the case of anomalous dispersion, $|b(\xi)| < 1$. The parameter E_d thus has to stay below the maximum carrier energy [14]:

$$\mathrm{MCE}[\Psi(\xi)] := \lim_{A\to(1/\sup_\xi|\Psi(\xi)|)^-} E[A\Psi(\xi)] \geq E_d. \tag{5}$$

The MCE has been observed to be finite for common carriers which result in time-limited signals [14, Sec. 2.4]. The duration of the generated signals can be manipulated by scaling the carrier $\Psi(\xi) \to \Psi(c\xi) \Rightarrow q(t) \to q(t/c)$, $c > 0$, [3, IV-D]. To keep utilizing the complete provided bandwidth, we

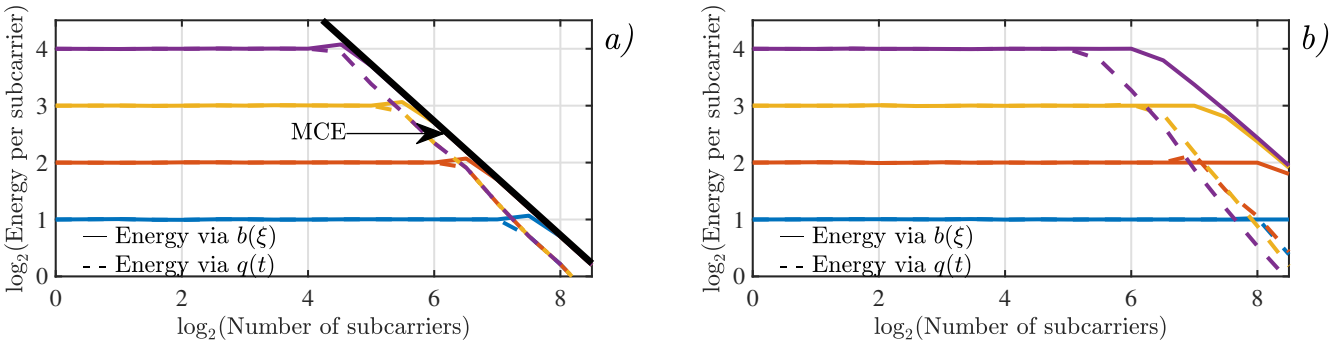

Fig. 1 *a)* PCCR: The two energy estimates agree almost upto the theoretical maximum. *b)* PCRB: The two estimates also start to decrease with number of subcarriers (signal duration) due to signal truncation and finite precision (similar to [12, Fig. 6a]).

choose $c_N = (2N+1)c_0$ and increase the number of subcarriers proportionally. We thus consider the following nonlinear spectrum

$$b_N(\xi) = \sum_{k=-N}^{N} s_k \Psi\left(c_N \xi - k\Delta_\xi\right) \tag{6}$$

in this paper. The generated signals have $2N+1$ subcarriers and are of duration $T_N = (2N+1)T_0$. The bandwidth stays approximately constant because the subcarriers shrink with N.

3 Theoretical Analysis

In this section we analyze how the maximum power that the b-modulator discussed in the previous section can achieve depends on the number of subcarriers, which is directly proportional to the signal duration. Our analysis rests on two simple insights. First, since the signals are of finite duration, energy translates directly into power. Second, since $E[\Psi(c_N\xi)] = c_N^{-1} E[\Psi(\xi)]$ by basic integration laws,

$$\mathrm{MCE}[\Psi(c_N\xi)] = c_N^{-1}\mathrm{MCE}[\Psi(\xi)]. \tag{7}$$

We bound the average power P_N achieved with $2N+1$ subcarriers using (4), (5), (7) and $c_N = (2N+1)c_0$:

$$\begin{aligned} P_N &= \frac{\mathbb{E}\{E[b_N(\xi)]\}}{T_N} \approx \frac{(2N+1)E_d}{T_N} \\ &\leq \frac{(2N+1)\mathrm{MCE}[\Psi(c_N\xi)]}{T_N} = \frac{c_0^{-1}\mathrm{MCE}[\Psi(\xi)]}{T_N}. \end{aligned} \tag{8}$$

Note that the numerator is a constant independent of the number of subcarriers, so that the bound on the transmit power P_N decreases with the signal duration T_N. To the best of our knowledge this is the first bound on transmit power ever reported for a NFDM system. We will observe in the simulation results that instructing the algorithms to achieve powers beyond this bound leads to numerical failure and rapidly decaying system performance. Hence our bound strongly suggests that for any signal duration T_N there is a finite optimum transmit power. We remark that even though our analysis holds for the particular b-modulation scheme in [14], similar observations have been reported also for other NFDM architectures [9–11].

4 Simulations

The goal of this section is two-fold. First, we demonstrate that our theoretical bound is useful to describe actual system behavior. Second, we compare the analyzed PCCR approach from Sec. 2 with an alternative scheme from [15] that we call power control by reshaping $b(\xi)$ (PCRB). The advantage of PCRB is that – in theory – arbitrarily large energies can be achieved. The disadvantage is that the generated signals are not of finite duration anymore. We want to investigate whether in practice PCRB can generate higher signal powers than PCCR.

Setup: We used the carrier waveform [14, (18)] with $T = 0.5$ for both systems. We chose the constants c_0, T_0 and Δ_ξ from Sec. 2 as 1.0, 0.5 and 135 respectively. The signals generated using PCRB were truncated to duration T_N. The signals generated using PCCR were of duration T_N by design. The symbols s_k were drawn from a QPSK constellation. The simulations were carried out using NFDMLab [16], which uses the software library FNFT [17] to compute (inverse) NFTs. To avoid algorithm breakdowns, all $b(\xi)$ were clipped such that $|b(\xi)| \leq 1 - 2.2204 \times 10^{-15}$. Furthermore a numerical improvement to the inverse NFT (INFT) described in the appendix was used. The fiber parameters were $\beta_2 = -5 \times 10^{-27}$ s^2/m, $\gamma = 1.2 \times 10^{-3}$ (Wm)$^{-1}$ and $\alpha = 2 \times 10^{-4}$ m^{-1}. The signal duration in real-world units was $1.25T_N$ ns. The transmitted and received signals were low-pass filtered to 40GHz. Amplification was carried out using EDFAs with a 6dB noise figure.

Impact of finite precision: Recall that the energy of the signal can be computed from $b(\xi)$ via (2) or from $q(t)$. Since $b(\xi)$ is the input to the INFT and $q(t)$ is the output, we compare these two energies in order to assess the accuracy of the INFT. In Fig. 1, we show the average signal energy (taken over 20 signal realizations) divided by the number of subcarriers for both PCCR and PCRB. In Fig. 1a we see that both energy estimates stay close together which hints that numerical effects in the INFT are not the major limiting factor for PCCR. In Fig. 1b we see that the energy via $b(\xi)$ eventually starts decreasing even though it should stay constant in theory. This behavior is due to the clipping mentioned above. The gap to energy via $q(t)$ is larger than in Fig. 1a, which we attribute to the signal

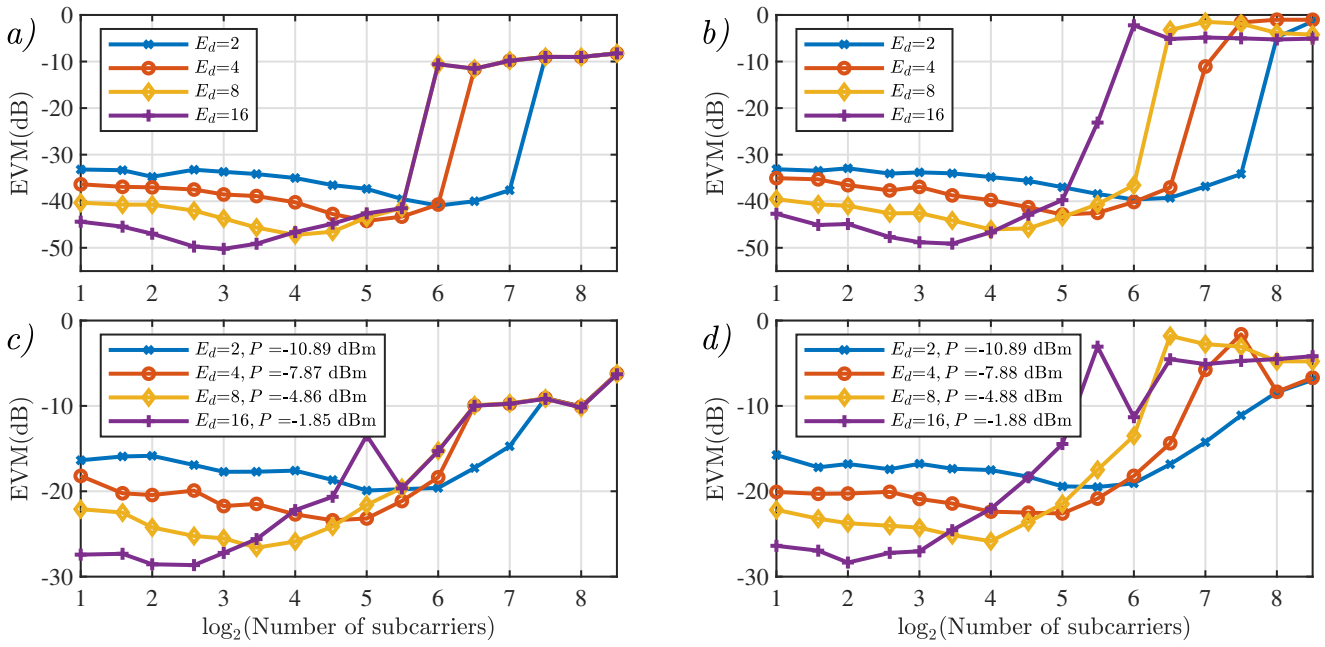

Fig. 2. *a)* B2B for PCCR *b)* B2B for PCRB *c)* Transmission for PCCR *d)* Transmission for PCRB

truncation mentioned above. The energies via $q(t)$ in Fig. 1b are higher than those in Fig. 1a but show a similar decay.

Back-to-back (B2B): We simulated 1m of fiber followed by a single amplifier to add noise. After demodulation and equalization, estimates $\hat{s}_k$ of the transmitted symbols s_k were obtained. For PCCR, error vector magnitudes (EVMs) between $\hat{s}_k$ and s_k were computed. For PCRB the inverse of the map $R(u) = \sqrt{1-e^{-|u|^2}}e^{i\angle u}$ [15, Fig. 2a] was applied to $\hat{s}_k$ before computing the EVM. This was done to ensure similarly shaped noise balls. The results are shown in Figs. 2a-b. In Fig. 2a, PCCR eventually breaks down due to ill-conditioning in the INFT algorithms. However, this happens only when trying to exceed the theoretical limit depicted in Fig. 1a. The initial decay of the curves seems to be a result of the nonlinear nature of the NFT which squeezes the noise balls [18, Fig. 2]. From Fig. 2b we observe that PCRB performs better than PCCR at low subcarrier energies but worse at the high one.

Transmission: We finally compared PCCR and PCRB in a transmission scenario. To make the scenario more realistic, we added precompensation as in [9, 11] and truncated the signals to $0.556T_N$ ns before transmission so that now both methods suffer from truncation errors. The signals were transmitted over a 8×80 km link. The results are shown in Figs. 2c-d. By comparing Figs. 2a and 2c, we observe that the breakdowns still occur approximately for the same number of subcarriers, which hints that the transmit power limitation from our theoretical analysis is a dominant effect even in our transmission setup. The spike in the $E_d = 16$ curve seems to occur due to numerical issues. We remark that it occurs when the maximum number of subcarriers for this E_d has been exceeded. Similar observations can be made when comparing Figs. 2b and 2d.

5 Conclusion

We derived an upper bound on the achievable transmit power for the b-modulator from [14] (PCCR) that decreases with signal duration for fixed bandwidth. It seems to be the first such bound for NFDM. In simulations we achieved transmit powers close to the theoretical bound which suggests that – in our setup – numerical signal-noise interactions were a minor issue. We found that another b-modulator from [15] (PCRB) suffers from similar limitations even though the maximum carrier energy argument used in our analysis does not apply to that case. We plan to use our analysis to improve NFDM system designs.

Acknowledgements This project has received funding from the European Research Council (ERC) under the European Unions Horizon 2020 research and innovation programme (grant agreement No 716669).

Appendix The INFT was computed as described in [13] with FNFT [17]. To run the algorithm we require D samples of

$$B(\tau) = \frac{1}{2\pi}\int_{-\infty}^{\infty} b(\xi)e^{i\tau\xi}d\xi \approx \frac{e^{i\tau\xi_-}}{2\pi}\int_{\xi_-}^{\xi_+} b(\xi)e^{i\tau(\xi-\xi_-)}d\xi \tag{9}$$

on a grid $\tau_k = \tau_- + k\delta$. We approximate the right integral by

$$\begin{aligned}\hat{B}(\tau_k) &= \frac{e^{i\tau_k\xi_-}}{2\pi}\sum_{n=0}^{M-1} b(\xi_n)e^{i\tau_k(\xi_n-\xi_-)}\epsilon \\ &= \frac{\epsilon e^{i\tau_k\xi_-}}{2\pi}\sum_{n=0}^{M-1} b(\xi_n)(e^{i\tau_-\epsilon}(e^{i\delta\epsilon})^{-k})^{-n},\end{aligned} \tag{10}$$

where $\xi_n = \xi_- + n\epsilon$. The $B(\tau_k)$ are computed fast by applying chirp z-transform [19] to the last sum.

6 References

[1] Zakharov, V. F. and Shabat, A. B.: 'Exact Theory of Two-dimensional Self-focusing and One-dimensional Self-modulation of Wave in Nonlinear Media', Journal of Experimental and Theoretical Physics, 1972, 34(1), pp. 62.

[2] Agrawal, G.: 'Nonlinear Fiber Optics', Academic Press, 2012, 5th edn.

[3] Yousefi, M. I. and Kschischang, F. R.: 'Information Transmission Using the Nonlinear Fourier Transform, Part I: Mathematical Tools', in IEEE Transactions on Information Theory, 2014, 60(7), pp. 4312-4328, DOI: 10.1109/TIT.2014.2321143

[4] Prilepsky, J. E., Derevyanko, S. A., Blow, K. J., et al.: 'Nonlinear Inverse Synthesis and Eigenvalue Division Multiplexing in Optical Fiber Channels', Physical Review Letters, 2014, 113(1), DOI: 10.1103/PhysRevLett.113.013901

[5] Turitsyn, S. K., Prilepsky, J. E., Le, S. T., et al.: 'Nonlinear Fourier transform for Optical Data Processing and Transmission: Advances and Perspectives', Optica, 2017, 4(3), pp. 307-322, DOI:10.1364/OPTICA.4.000307

[6] Le, S. T., Aref, V. and Buelow, H.: 'Nonlinear Signal Multiplexing for Communication Beyond the Kerr Nonlinearity Limit', in Nature Photonics, 2017, 11, DOI: 10.1038/nphoton.2017.118

[7] Gaiarin, S., Perego, A. M., da Silva, E. P., et al.: 'Dual-polarization Nonlinear Fourier Transform-based Optical Communication System', Optica, 2018, 5(3), pp. 263-270, DOI:10.1364/OPTICA.5.000263

[8] Goossens, J.-W., Yousefi, M. I., Jaouën, Y., et al.:, 'Polarization-division Multiplexing based on the Nonlinear Fourier Transform', Optics Express, 2017, 25(22), pp. 26437-26452, DOI:10.1364/OE.25.026437

[9] Civelli, S., Forestieri, E. and Secondini, M., 'Why Noise and Dispersion May Seriously Hamper Nonlinear Frequency-Division Multiplexing' in IEEE Photonics Technology Letters, 2017, 29(16), pp. 1332-1335, DOI: 10.1109/LPT.2017.2722040

[10] Le, S. T., Aref, V. and Buelow, H.: 'High Speed Precompensated Nonlinear Frequency-Division Multiplexed Transmissions', in Journal of Lightwave Technology, 2018, 36(6), pp. 1296-1303, DOI: 10.1109/JLT.2017.2787185

[11] Le, S. T. and Buelow, H.: 'High Performance NFDM Transmission with b-modulation', Photonic Networks, 19th ITG-Symposium, Leipzig, Germany, 2018, pp. 1-6.

[12] Yangzhang, X., Le, S. T., Aref, V., et al.: 'Experimental Demonstration of Dual-polarisation NFDM Transmission with b-Modulation', in IEEE Photonics Technology Letters, 2019, DOI: 10.1109/LPT.2019.2911600

[13] Wahls, S.: 'Generation of Time-Limited Signals in the Nonlinear Fourier Domain via b-Modulation', Proc. European Conf. Optical Comm. (ECOC), Gothenburg, 2017, pp. 1-3, DOI: 10.1109/ECOC.2017.8346231

[14] Gui, T., Zhou, G., Lu, C., et al.: 'Nonlinear Frequency Division Multiplexing with b-modulation: Shifting the Energy Barrier', Optics Express, 2018, 26, pp. 27978-27990, DOI:10.1364/OE.26.027978

[15] Yangzhang, X., Aref, V., Le, S. T., et al.: 'Dual-Polarization Non-Linear Frequency-Division Multiplexed Transmission With b-Modulation', Journal of Lightwave Technology, 2019, 37, pp. 1570-1578, DOI:10.1109/JLT.2019.2902961

[16] Brehler, M., Mahnke, C., Chimmalgi, S., et al.: 'NFDMLab: Simulating Nonlinear Frequency Division Multiplexing in Python', in Proc. of Optical Fiber Comm. Conf. (OFC), San Diego, 2019, paper M3Z.13, DOI:10.1364/OFC.2019.M3Z.13

[17] Wahls, S., Chimmalgi, S. and Prins, P. J.: 'FNFT: A Software Library for Computing Nonlinear Fourier Transforms', Journal of Open Source Software, 2018, 3(23), 597, DOI:10.21105/joss.00597

[18] Wahls, S.: 'Second Order Statistics of the Scattering Vector Defining the D-T Nonlinear Fourier Transform', SCC 2017, 11th International ITG Conference on Systems, Communications and Coding, Hamburg, Germany, 2017, pp. 1-6.

[19] Rabiner, L., Schafer, R. and Rader, C.: 'The Chirp Z-transform Algorithm', IEEE Transactions on Audio and Electroacoustics, 1969, 17(2), pp. 86-92, DOI: 10.1109/TAU.1969.1162034